

4.1) Introduction

In order to have confidence in the accuracy of the numerical solutions provided by simulation software, experimentation is required to determine the sensitivity of the numerical parameters. Because of limited resources, physical experimentation could not be conducted in this work, but simulation results were compared with a manufactured waveguide structure as presented in [1].

4.2) Selection of the waveguide class

As was seen in chapter 3, there are various choices when selecting a waveguide to use in a design, but knowing beforehand what devices will be designed aids in the selection process. After investigating various waveguide structures, ranging from silica to sol-gel, the choice fell on the SiON waveguide presented in [1]. The first consideration was that the index difference between the cladding and core regions is in excess of 3%, making these waveguides most suitable for designing components utilising small bending radii, such as directional couplers and AWGs. The penalty for this will be higher insertion losses due to modal mismatch at the coupling interface. Compensation is done by spot size converters as shown in [2]. The waveguides exhibit low losses, making the manufacturing of Mach-Zehnder lattice filters (which can be centimetres long) a possibility. These waveguides also display polarisation insensitivity, which is especially favourable if AWGs are to be designed. Another consideration is that the ECR-PECVD process used to manufacture these waveguides is available in our laboratories [3], enabling future manufacturing work to be done that builds on the designs in this thesis.

4.3) Simulation setup

A suitable and reliable way of manufacturing passive waveguides is presented in [1]. It involves the deposition of silicon oxynitride (SiON) layers onto a cladding of SiO₂, as depicted in figure 4.1. The deposition of SiON layers is an excellent technique for

creating waveguide structures, mainly because of the fact that the refractive index profile can be varied over a wide range of values [1,2,3].

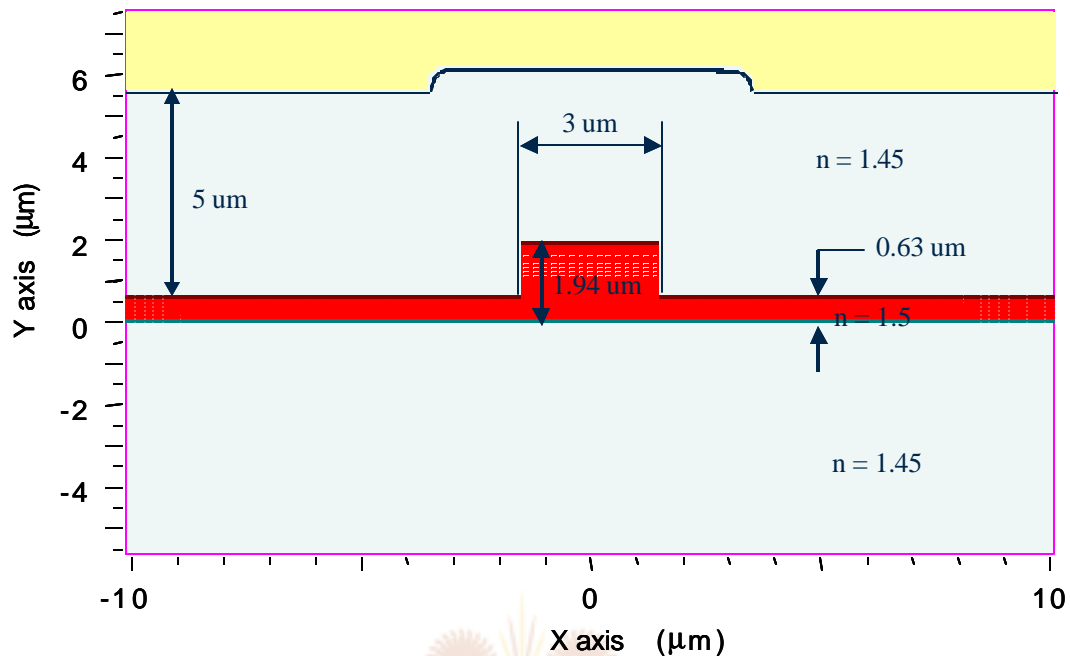


Figure 4.1: Profile of rib waveguide used in simulations

The SiON layers (core of 1.5 and over-cladding of 1.45) depicted in the above figure are deposited by means of an Oxford system 100 PECVD tool, whereas the thicker lower cladding of 1.45 (in excess of 9μm) layer is formed by thermal oxidation. The substrate comprises of a 4-inch ($\pm 100\text{mm}$) silicon <100> wafer. A detailed description of the manufacturing method and process is given in [1].

The waveguide as presented here has an index contrast of $\Delta = 100 \times ((1.5^2 - 1.45^2)/(2 \times 1.5^2)) = 3.28\%$. The important results from [1], in terms of the simulation of the waveguides, are the propagation loss, birefringence, thermo-optic coefficient, final dimensions and final refractive indexes of the optical layers. The *final* dimensions and *final* refractive indices are mentioned because an annealing process is included in the manufacturing process to improve the loss characteristics of the waveguides. The values for the abovementioned parameters were found to be [1]:

- 1) Propagation loss: The loss in the region between 1545 and 1565 nm has an average value of 0.15 ± 0.05 dB/cm.
- 2) Birefringence: Values in the order of less than 1×10^{-4} , making this parameter negligible for simulation purposes. This low value was obtained by etching deep trenches alongside the waveguides, and through optimisation of the deposition and annealing steps. These waveguides can thus be applied in filtering architectures because of their polarization independence.
- 3) Final dimensions: The average layer thickness measured from 3 runs is found to be $1.9498\mu\text{m}$ after annealing. This constitutes a decrease of 10% in thickness.
- 4) Final refractive indices: The average core refractive index measured from 3 runs is found to be 1.5172 after annealing, whereas the average cladding refractive index at 632.8 nm is 1.4571. This constitutes an increase of 1.2% in the refractive index between the pre and post annealed waveguides.
- 5) Thermo-optic coefficient: The measured effective index of the layer is $dN_{\text{eff}}/dT = 1.2 \times 10^{-5} \text{ } ^\circ\text{C}^{-1}$. The use of this parameter will be described in the section covering the simulation results for a tuneable MZI coupler.

It is important to note the increase in refractive index and decrease in layer thickness. These changes should be compensated for when deposition of the core and over-cladding layers is done in such a way that the final values correspond to the design specifications.

To incorporate the propagation loss in the BeamPROP environment, the measured values need to be translated in order for the software to use it. BeamPROP includes losses in the circuit by means of a parameter called α (this α is not the same as defined in chapter 2), which relates to the imaginary coefficient of the refractive index. It represents the material loss of the waveguide core. In terms of γ (denoted in chapter 2 by α), the usual loss coefficient (given in units of per μm), the imaginary index is given by:

$$\mathbf{a} = \frac{\mathbf{gl}}{4\mathbf{p}} \quad (4.1)$$

In view of equation 4.1, it can be shown that $\alpha = 1.2053 \times 10^{11}$. This value was obtained by expressing 0.2dB/cm as 0.9772/cm by using $\text{dB} = -20\log(\text{value})$. Expressed in units of per μm it becomes $9.772 \times 10^{-5}/\mu\text{m}$, and substitution of this value for γ together with $\lambda = 1.55\mu\text{m}$ in equation 4.1 yields the value for alpha.

All of the above values can be specified in the BeamPROP CAD environment for simulation purposes.

4.4) Mode field simulations

Simulations are first performed on a straight waveguide segment to characterize it in terms of the fundamental mode, mode field radius, insertion loss and total number of modes. The mode field radius is defined as the radius of the Gaussian approximation to the mode where the irradiance has fallen to $1/e^2$ (13.5%) of its axial value. Insertion loss is defined as the ratio of the power output of the device (P_{out}) to the power into the device (P_{in}) at one wavelength, one input state of polarization, and typically for the fundamental mode of the waveguide.

The simulated fundamental mode is depicted in figure 4.2. It should be noted that a TE polarization was used with a wavelength of 1550nm. The mode field diameter can be read off the figure, as $3.1\mu\text{m}$ in the x direction and $2.2\mu\text{m}$ in the y direction, as indicated by the block in figure 4.2. The slight deformation effect of the slab region on the Gaussian shape is clearly visible in figure 4.2. It is also instructive to view the mode on a 3D axis, as depicted in figure 4.3. The Gaussian shape of the propagating pulse is evident from this graphic representation.

By launching the fundamental mode into the waveguide and monitoring the power, the insertion loss for a 1cm waveguide is found to be 0.0126dB. A fibre mode was also launched into the waveguide, which yielded an insertion loss of 0.7dB at the launch interface. The fibre mode has characteristics matching the waveguide, and not any specific commercial fibre. It indicates the mode mismatch from a cylindrical waveguide to a square one.

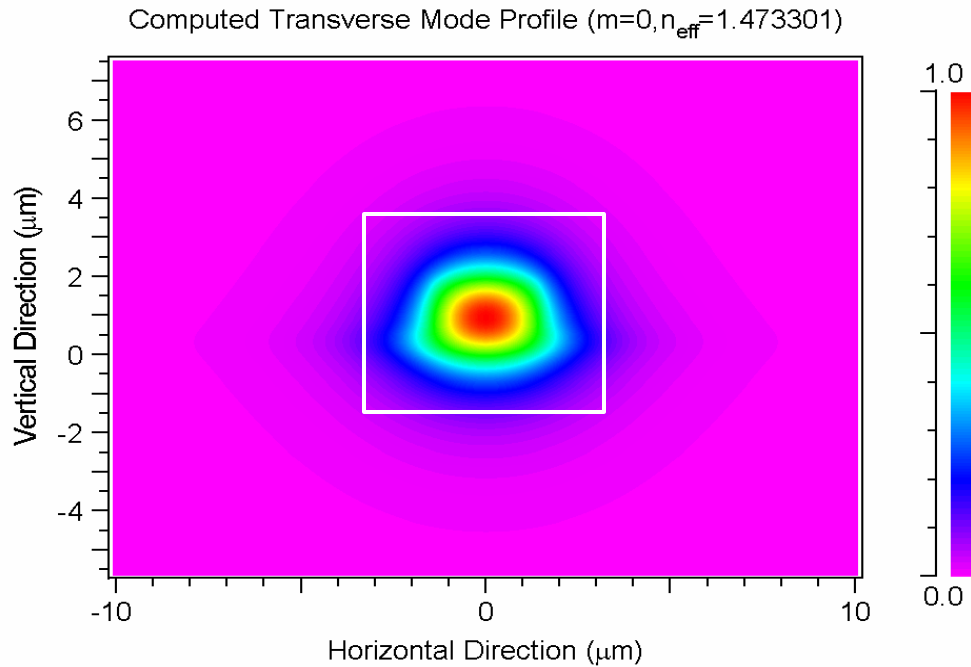


Figure 4.2: View of the fundamental mode in the XY-axis. The colour bar represents the normalised light intensity.

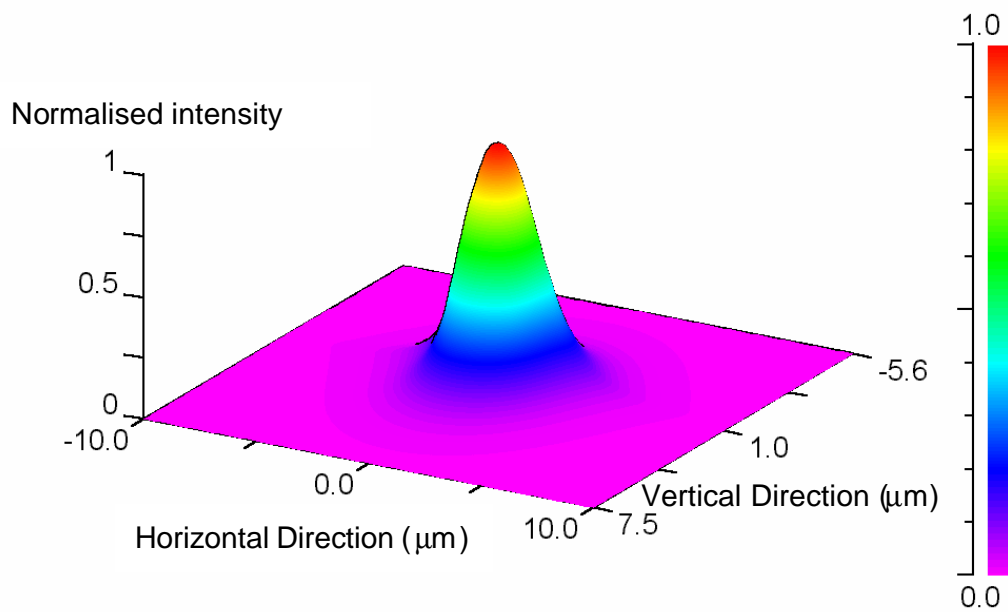


Figure 4.3: Three -dimensional view of the fundamental mode. The colour bar represents the normalised light intensity.

4.5) *Bend loss simulations*

The next step is to characterise the waveguides in terms of the bending loss related to radius of curvature. With these results, optimal offsets and radii can be chosen for the specific waveguide system.

To obtain the optimized parameters, two methods may be used, namely the direct beam propagation method or the simulated bend method. Although direct BPM allows for the most straightforward approach, there are drawbacks when implementing it. These are:

- 1) Direct simulation of curved waveguides with large angles (i.e. angles $> 1.2^\circ$) tend to be inaccurate, even with Padé-based wide angle methods
- 2) It is not always clear what properties should be monitored in the simulation environment.

The simulated bend method has no limitation on the bend angle, because it makes use of a coordinate transformation to map the curved waveguide onto a straight one. It should be noted that the method is accurate when the waveguide width \ll radius of curvature (smaller than 1%). Furthermore, by using the simulated bend method, the modes in the bend region can be compared in order to achieve loss minimization.

To obtain simulation data for the curved waveguides the bend radius is set for each test and the arc length calculated for that specific system. Next, the fundamental mode is obtained and launched into the same waveguide in order to monitor the loss of power in terms of the fundamental mode. This step facilitates the calculation of the mode overlap for the waveguide. The input angle is chosen to be 0° , whereas the output angle is 180° , as indicated in figure 4.4. A block diagram describing the process is also presented in figure 4.4.

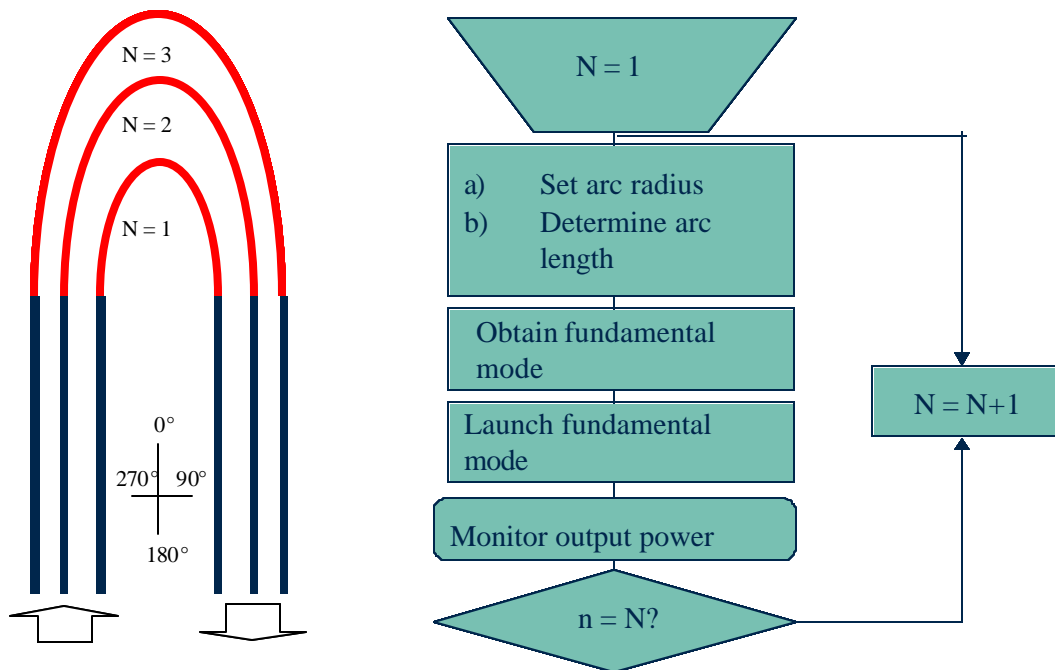


Figure 4.4: Procedure summary for bend-loss simulations

In figure 4.5 the BeamPROP simulation results are presented. The exponential decay in transmission as discussed in section 2.7.3 is evident here. Because of the exponential nature of the loss curve, a safety factor has to be incorporated in our selection of the minimum bending radius in order to ensure that manufacturing anomalies aren't detrimental to the manufactured component. Bearing this in mind, figure 4.6 shows a detail of figure 4.5 starting from the bending radius of 1.1mm. The reader will immediately notice the increase in loss as the radius increases – quite contradictory to what we expect. We have to remember, however, that the arclengths between each radius jump is in the order of 314 μ m, introducing the observed losses. With this in mind, an absolute minimum bending radius of 1.4mm is chosen. This ensures that if the patterning process yields a bending radius of 1.3mm for example, the losses will still be within acceptable bounds.

The above results are in excellent agreement with the minimum bending radius of 1.5mm obtained in [1]. The sensitivity of the simulation program to the input parameters varies with step sizes and numerical schemes. From these compared results it is clear that the simulation schemes are being used correctly.

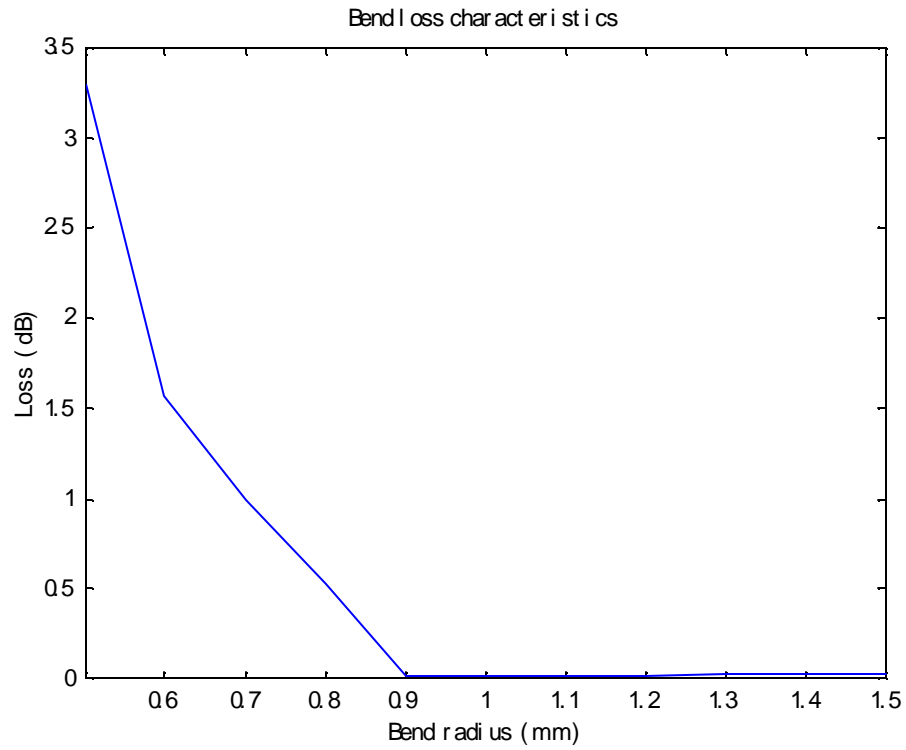


Figure 4.5: Bend loss characteristics

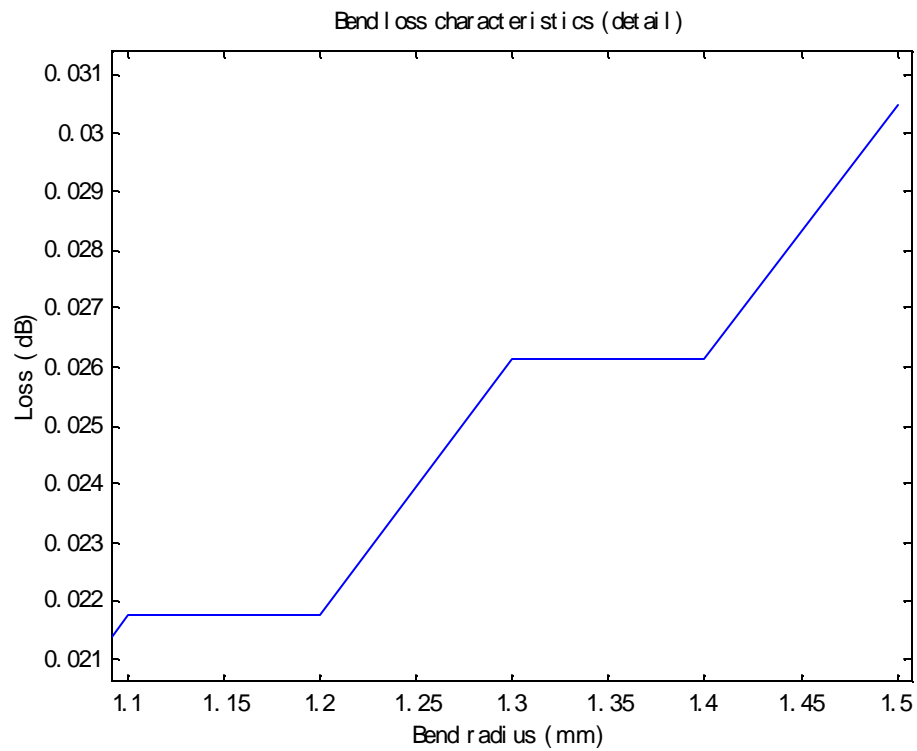


Figure 4.6: Detail of bend loss characteristics

4.6) Offset determination for loss optimization

In order to limit the mode mismatch in regions where the bending radius changes abruptly (for example at the interface where a straight waveguide section and a curved waveguide section meet), simulations were run to obtain the offsets required to minimize these losses. This is done by launching the fundamental mode of the first waveguide section into the second waveguide section while varying the lateral offset of the input mode, and calculating the mode field overlap between the two modes. The maximum value of this calculation corresponds to the optimal offset point.

In figure 4.7 it can be seen that an offset of $\pm 0.1\mu\text{m}$ to the right can be used to minimize loss from a straight to a curved waveguide (with a radius of 1.5mm). This offset is a very small and becomes negligible in the manufacturing process. A simulation with a finer increment of offset may be run to calculate the offset more accurately if necessary. For the interface corresponding to a straight waveguide to a curve with a negative radius of figure 4.7, the required offset will move to the left.

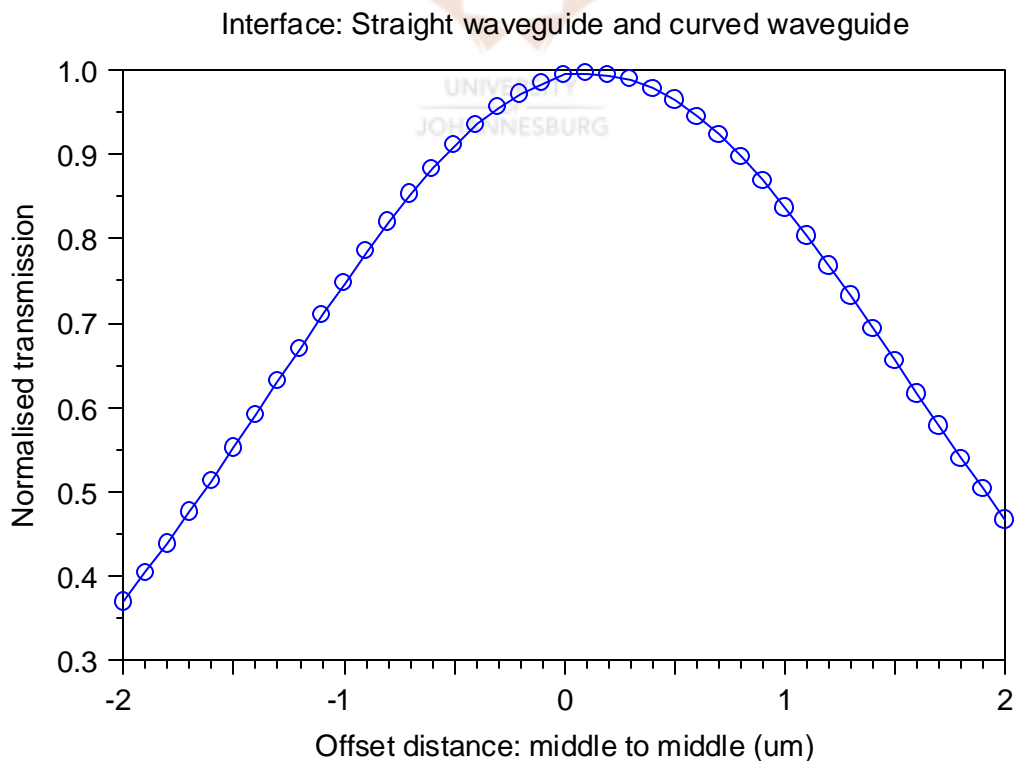


Figure 4.7: Interface between straight and curved waveguide

4.7) Conclusion

The simulation for an actual manufactured waveguide structure was presented. The results correlate very well with the measured values presented in [1], indicating that the simulation program treats the input variables with the correct sensitivity. Simulations are valuable initially as first-order approximations, and also as optimisation tools once a design has been validated through experimental physical testing.

4.8) References

- 1) R. Germann, H.W.M. Salemink, R. Beyeler, G.L. Bona, F. Horst, I. Massarek, B. Offrein, "Silicon oxynitride layers for optical waveguide applications", *Journal of the Electrochemical Society*, vol. 147, no. 6, pp. 2237-2241, 2000.
- 2) R. de Ridder, K. Worhoff, A. Driesen, P. Lambeck, H. Albers, "Silicon oxynitride planar waveguideing structures for application in optical communication", *IEEE Journal of Selected Topics in Quantum Electronics*, vol. 4, pp. 930 – 937, 1998.
- 3) P.V. Bulkin, "Electron cyclotron resonance plasma enhanced chemical vapour deposition of SiO_xN_y : Optical Properties and Applications", Rand Afrikaans University, Doctoral Thesis, 1994.